Ultrahigh-vacuum quasiepitaxial growth of model van der Waals thin films. II. Experiment

S. R. Forrest, P. E. Burrows, E. I. Haskal,* and F. F. So†

Advanced Technology Center for Photonics and Optoelectronic Materials (ATC/POEM), Department of Electrical Engineering, Princeton University, Princeton, New Jersey 08544

(Received 24 November 1993)

We study the growth of the archetypal planar molecular compounds; 3,4,9,10 perylenetetracarboxylic dianhydride 3,4,7,9 naphthalenetetracarboxylic dianhydride, and copper phthalocyanine on a variety of substrates by the ultrahigh-vacuum process of organic molecular-beam deposition. The thin-film structures are grown as monolayers, multilayers, alternating thin-film stacks (or multiple quantum wells), and bulk thin films with thicknesses extending to 4000 Å. Techniques used to investigate these structures include scanning tunneling microscopy, *in situ* reflection high-energy electron diffraction, electron microscopy, x-ray diffraction, and optical and electronic characterization. We find that highly ordered crystalline thin-film growth (i.e., quasiepitaxy) can often be achieved independent of the commensurability of the grown layer and the substrate. Such structural ordering is shown to strongly influence both the optical and electronic properties of the films. The structures experimentally determined for these film systems are consistent with the theoretical predictions made in paper I, where we analyze films consisting of large planar organic molecules bonded by van der Waals forces. These results provide evidence for the generality of quasiepitaxial growth of such molecular thin-film systems.

I. INTRODUCTION

In paper I, we presented a detailed theoretical framework for the widely observed phenomenon of the quasiepitaxial growth of organic thin films.[1] In particular, these calculations considered purely van der Waals (vdW)-bonded planar molecules, of which 3,4,9,10 perylenetetracarboxylic dianhydride (PTCDA) and 3,4,7,8 naphthalenetetracarboxylic dianhyrdride (NTCDA) are archetypes. The theory is based on extensive experimental evidence that these molecules do indeed grow into approximately ordered crystalline structures which we have presented in past work. In this paper, we summarize several key experimental results published previously concerning the microstructure of thin films of these compounds. In addition, we present results which provide further evidence of the crystalline order of the compounds deposited in both monolayer and multilayer thin-film stacks using the ultrahigh-vacuum process of organic molecular-beam deposition of (OMBD). The film structures, along with those obtained for copper phthalocyanine (CuPc) are then compared with our theoretical modeling results. Agreement between predicted and observed structures is found to be good, thereby confirming some of the more fundamental aspects of the theory presented in paper I.

The methods used to determine the film microstructure and discussed in this paper include scanning tunneling microscopy (STM), *in situ* reflection high-energy electron diffraction (RHEED), x-ray diffraction, electron microscopy, and optical measurements.

The bulk structures of the molecules studied are provided in paper I (Sec. II). In this paper, we consider the growth of monolayer and multilayer stacks, as well as the bulk film properties. We begin in Sec. II with a description of the OMBD deposition system as well as the molecular source purification and deposition conditions. In Sec. III, we use STM to image a monolayer of PTCDA grown on highly oriented pyrolytic graphite (HOPG). The evolution of crystalline order from a monolayer to bulk PTCDA, and subsequently to multilayer stacks of PTCDA on NTCDA and PTCDA on CuPc on graphite substrates, is examined by RHEED in Sec. IV. In Sec. V, we study the effects of substrate temperature on film morphology and crystalline order using a combination of x-ray diffraction and carrier mobility measurements. In Sec. VI, we consider bulk film dielectric and conductive properties of quasiepitaxially (QE) grown thin films consisting of PTCDA on a variety of substrates. Finally, in Sec. VII we summarize our results and compare them with predictions of the theoretical model presented in paper I.

II. SAMPLE PREPARATION AND GROWTH

A. Organic source material purification

Commercially available[2] PTCDA, NTCDA, and CuPc were purified using gradient sublimation[3] prior to loading the source materials into the ultrahigh-vacuum deposition system. Typically, several grams of powdered source material are loaded into the end of a 60-cm-long glass tube. A glass sleeve is then placed inside the tube to capture the sublimed material, followed by a wad of glass wool placed at the open end of the tube to prevent the source material from contaminating the pumping chamber. The tube is evacuated to 1×10^{-6} Torr, and the end containing the organic source material is inserted into a furnace. The temperature of the furnace is gradually increased until the sublimation point of the material is reached (approximately 400 °C for PTCDA, 210 °C for NTCDA, and 300 °C for CuPc), a process typically taking

several days. Purified organic crystals grow on the inside wall of the glass sleeve in the warm zone of the furnace, while more volatile impurities are evacuated. Nonvolatile impurities are left at the hot end of the glass tube. The glass sleeve insert is removed, and the crystals are removed to be used as the source material for the second purification cycle. Before loading the source materials into the UHV system, all organic compounds are purified three times using this method. The purified materials are loaded immediately into the OMBD effusion cells, where they are continuously maintained in ultrahigh vacuum at a temperature slightly less than their sublimation temperature. Work in our laboratory and elsewhere[4] has shown that the use of UHV deposition conditions and material storage is important in achieving high quality crystalline film growth. For example, monolayer growth without island clumping is observed by scanning tunneling microscopy only for films deposited under UHV conditions. We speculate that the UHV storage of the source material at elevated temperatures is a key factor in eliminating impurities and moisture which lead to film defects during growth.

B. Deposition and growth

The ultrahigh-vacuum chamber used for organic molecular-beam deposition is shown schematically in Fig. 1. The system base pressure is $<1\times10^{-10}$ Torr, achieved using a combination of cryo, ion, and Ti sublimation pumping. Liquid-nitrogen-cooled shrouds surround the growth area as well as the top of the effusion cells to prevent outgassing and molecular cross contamination of the source material. Prior to growth, a substrate is mounted onto a copper block using either indium solder or spring clips. The samples are introduced into the high-vacuum environment through a load lock, and are mounted on a sample manipulator whose temperature can be varied continuously from 80 to 900 K. As will be discussed below, the lower temperatures are required to achieve crystalline growth of PTCDA and NTCDA, and the highest temperatures are used for substrate bakeout prior to growth. The substrate manipulator also allows for continuous sample rotation via mounting through a differentially pumped rotary feedthrough. Substrate temperature is controlled using a thermocouple/boron nitride heater combination which is connected to the control electronics via a low-noise, rotary slip ring.

The rate of thin-film deposition is controlled by heating the powdered source material in a Knudsen cell positioned approximately 25 cm from the substrate holder. The deposition rate and film thickness is measured with a quartz-crystal thickness monitor located adjacent to the substrate, and is typically maintained at 0.1–0.5 Å/s for the thinnest films, and is increased to as high as 3 Å/s in growing 200–1000-Å thick films. Growth is terminated by closing the main shutter in front of the sample, followed by closing the Knudsen cell shutter and then cooling the cell to its standby temperature. The chamber pressure during growth ranges from 10^{-9} to 10^{-7} Torr, returning to the chamber base pressure of 10^{-10} Torr immediately after the growth sequence is completed.

III. SCANNING TUNNELING MICROSCOPY (STM) OF ORGANIC MONOLAYERS

Scanning tunneling microscopy has previously been shown to be capable of molecular resolution of organic molecules.[5–8] Ludwig *et al.*[7] presented molecular resolution images of PTCDA deposited on HOPG held at 340–400 K. They explained their results in terms of a surface unit cell similar to the bulk unit cell, but 5–10 % larger. In contrast to the work presented here, their films were deposited under conditions different from those shown to produce crystalline layers of PTCDA and similar materials.[9–13] In the experiments described here, we

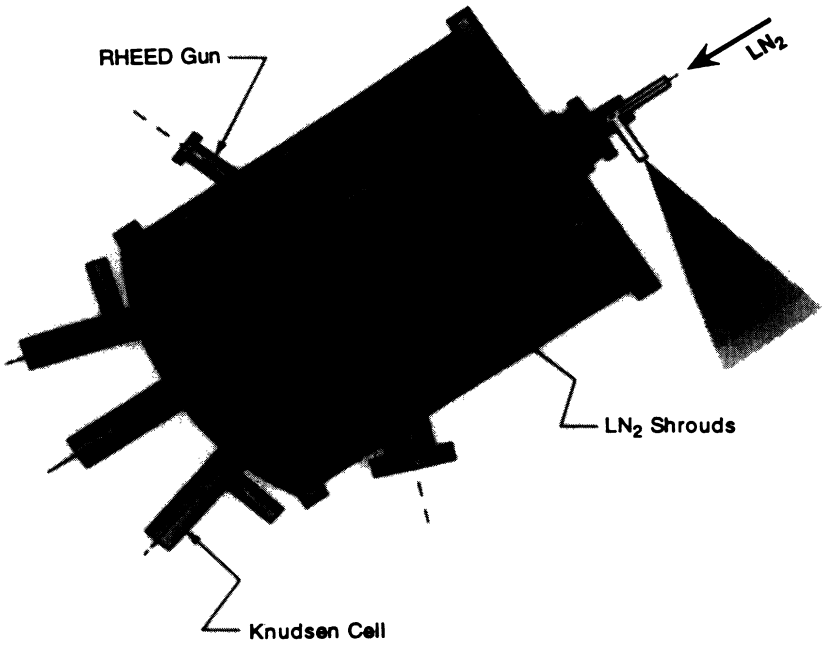

FIG. 1. Cross-sectional view of the organic molecular-beam deposition chamber. The rotating substrate holder can be temperature controlled between 80 and 900 K using a combination of liquid-nitrogen-cooling and boron-nitride-heating elements.

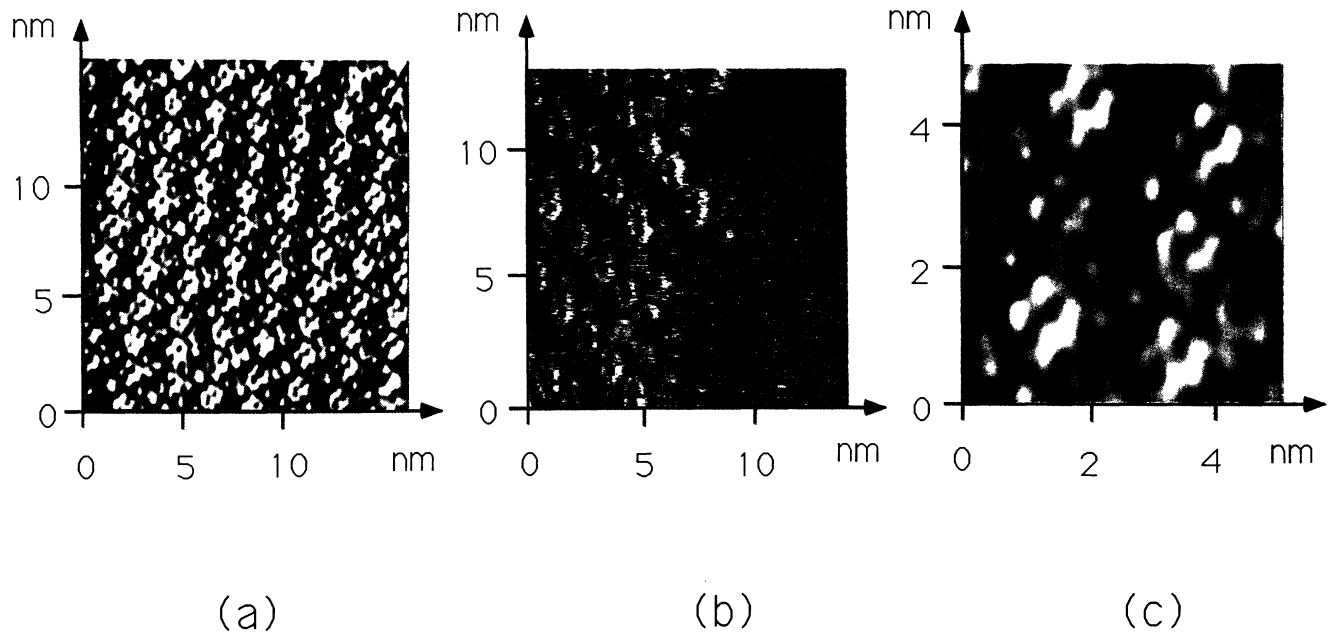

FIG. 2. (a) False color filtered STM image of crystalline PTCDA on HOPG. Tip operating parameters: 402.1-mV, 0.10-nA tip positive. (b) Unfiltered STM image of the edge of an island of PTCDA on HOPG. Tip operating parameters: 403.7-mV, 0.10-nA tip positive. (c) Detail of (a), showing the unit cell of PTCDA on HOPG.

use the STM to study the crystal structure at the onset of film growth by examining the first monolayer of PTCDA deposited by OMBD on HOPG substrates held at low temperature (90 K), and find that these results are consistent with those obtained by RHEED (see Sec. IV). We show that the surface unit cell is expanded from that found in the bulk, and the individual molecules are rotated from their equilibrium bulk configuration. Furthermore, we determine an orientational relationship between the PTCDA layer and the graphite substrate. Our interpretation of the STM image is supported by calculations presented in paper I, which minimize total crystal energy to determine the equilibrium positions of molecules within the two-dimensional unit cell of PTCDA.

Prior to film deposition, a 1.4-cm^2 HOPG substrate was cleaved in air and immediately loaded into the deposition chamber via a vacuum load lock mechanism. The substrate was heated to 900 K for 15 min in vacuum to desorb surface contaminants, and then cooled to 90 K immediately prior to film growth. The effusion (Knudsen) cell was heated to approximately 310 °C to achieve a PTCDA deposition rate of 0.1–0.2 Å/s. Approximately 4 Å (or approximately one monolayer) of PTCDA was deposited, as measured by a quartz-crystal thickness monitor. Such a measured thickness is consistent with the disappearance of the substrate diffraction streaks in the RHEED experiments (Sec. IV).

The deposited film was imaged in air using a commercial STM (Ref. 14), with controlled geometry Pt/Ir tips.[15] All images were obtained from samples within 24 h of their removal from the vacuum system. Current images (constant height mode) apparently showing single molecules of PTCDA were readily obtained on several samples at tunneling currents of ~0.1 nA and a tip voltage of ~400 mV, which was positive with respect to the substrate. No images were obtained with the tip biased negatively with respect to the substrate. A typical image, filtered to reduce noise, is shown in Fig. 2(a). Such images were stable for ~10–20 scans before disappearing, to be replaced by an image of the underlying graphite lattice. The loss of the PTCDA image is attributed to the weakly bound organic molecules being swept away by the tip, this interpretation being supported by the observation that higher tunneling currents result in a higher rate of image degradation.

Figure 2(b) shows a sample unfiltered image of the edge of an island of PTCDA; the individual molecules appear

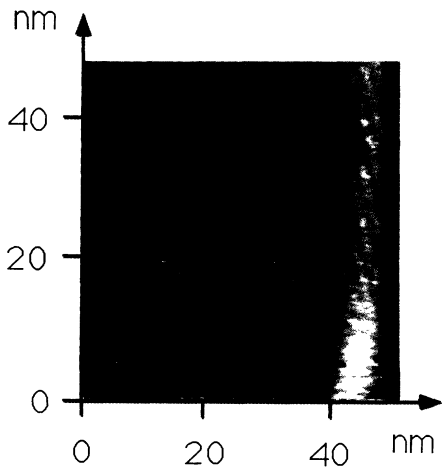

FIG. 4. STM image of two crystalline grains of PTCDA on a HOPG substrate. The space in the center of the "V" between the grains is a region where no PTCDA growth has occurred.

as broken double circles. Coupled with the high reproducibility of the images between numerous different samples, and using different tips, the observation of island edges provides evidence that the images presented are, in fact, of a monolayer of the organic thin film on graphite.

In a second series of experiments, PTCDA was deposited on graphite in a conventional, bell jar metal deposition system. This turbo-pumped system has a base pressure of 10^{-7} Torr, and the crystalline powder source materials are loaded into baffled, Mo boats prior to deposition. While it was found that high-resolution images of monolayer films such as those in Fig. 2 could always be obtained from films deposited using the UHV-OMBD system, no clear images could be obtained for similar films deposited in the bell jar system. Instead, thin films deposited in the lower-vacuum bell jar system appeared to clump into islands several monolayers in thickness. While we are not certain why this difference in film order is observed, we speculate that it is due to impurities incorporated during growth from the lower-vacuum apparatus, along with the presence of moisture in the source material. Given that some of the materials used are hygroscopic, water molecules may serve as crystal nucleation sites, leading to island growth. Maintaining the source material at elevated temperatures in UHV for long periods, as is done in the OMBD chamber, tends to eliminate moisture, resulting in higher-purity source material and hence higher quality monolayer films.

Based on the STM images in Fig. 2, we propose a model for the two-dimensional unit cell of PTCDA on HOPG shown in Fig. 3, with the measured dimensions and angles between the molecules listed in Table I. The linear dimensions a and b are measured and calibrated relative to an image of the HOPG lattice taken from approximately the same region of the substrate as the monolayer image. The angle σ is measured directly from the images taken from the several samples studied, whereas the angle ξ is measured using Fig. 2(c). This is a magnified detail of the unit cells in Fig. 2(a) showing the fifth, central, molecule of the unit cell, which is faintly apparent in the low magnification image as well. The positions of the long molecular axes are indicated by the line segments shown in the figure.

Lattice dimensions and angles measured from images of different samples with different tips are reproducible within the limits quoted in Table I. Two PTCDA molecules define a rectangular unit cell with dimensions $a=21.6\pm2.2$ Å and $b=15.2\pm1.6$ Å, in contrast to the bulk unit cell with dimensions $a=17.34$ Å and $b=11.96$ Å. The angles σ and ξ are 0.82 ± 0.07 ad 0.61 ± 0.17 rad, respectively. The two-dimensional lattice parameters are

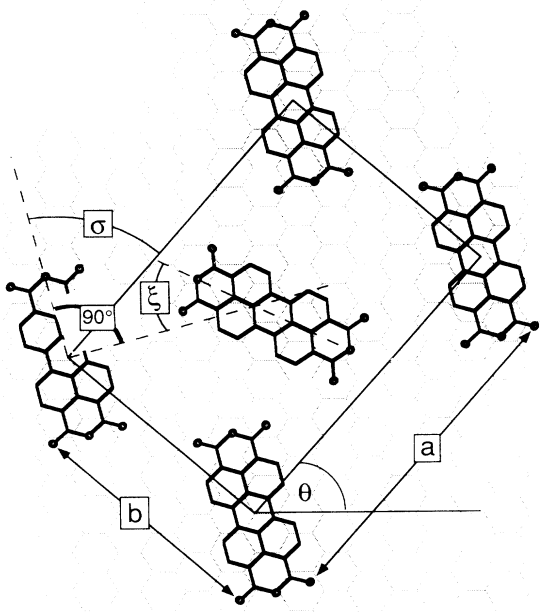

FIG. 3. Proposed structure for the two-dimensional unit cell of PTCDA on HOPG, showing the parameters measured and displayed in Table I.

in good agreement with those obtained using RHEED (Sec. IV), which are also listed in Table I for comparison with the STM data. The apparent removal of the organic molecules by the tip also allows us to examine the orientational relationship between the organic film and the graphite substrate. Here it is assumed that the area of graphite imaged after disappearance of the organic layer lies within the same crystal grain of graphite as the organic layer (i.e., within a few microns). From these images we obtain $\theta=0.82\pm0.17$ rad, which is the angle between the graphite and PTCDA lattices as shown in Fig. 3.

Scanning tunneling microscope images taken over larger fields of view show boundaries between two adjacent grains of PTCDA. A typical STM image over an area of 100 Å near such a grain boundary is shown in

TABLE I. PTCDA surface unit-cell parameters.

	a (Å)	b (Å)	σ (rad)	ξ (rad)	θ (rad)
Theory[a]	20.0±0.5	15.7±0.5	0.86±0.02	0.48±0.02	0.86±0.02
STM	21.6±2.2	15.2±1.6	0.96±0.03	0.61±0.17	0.82±0.07
RHEED	22.4±1.0	16.0±1.0			

[a]Reference 1.

Fig. 4. The angle between the PTCDA molecular axes measured in different grains is always observed to be an integer multiple of $\pi/3$ radians. Since the graphite substrate has sixfold-rotational symmetry, nucleating islands of PTCDA are energetically identical at rotations of $\pi/3$ radians with respect to the substrate.[1] The absence of any other angles in the observed STM images strongly suggests a preferred angle of orientation between the organic layer and the substrate. Note that this relative orientation between the PTCDA and graphite lattices is striking evidence for quasiepitaxial growth. That is, even though the two lattices are highly incommensurate, they align in a consistent fashion with respect to each other. This observation also points to a fundamental and obvious limitation of quasiepitaxy: If the symmetries of the two lattices are not identical, the deposited layer must contain high-angle grain boundaries between islands which have separately nucleated at different lattice sites.[1] Given that the monoclinic cells characteristic of many crystalline organic semiconductors have a twofold symmetry, achieving perfect or near-perfect film order is restricted to growth on substrates with similarly low symmetries.

From the STM data and from calculations in paper I, we infer that the enlarged reconstructed surface until cell is a direct result of the lack of vdW bonds extending above the top layer. This absence allows the cell to expand slightly to minimize the repulsive core energy between adjacent molecules. We note, however, that this surface reconstruction does *not* depend strongly on the substrate, but rather is a result of the comparatively strong *intermolecular* forces within the cell itself. An important question arises regarding the filling of vacancies as subsequent layers are grown on the low-density, reconstructed surface. Our measurements indicate that the surface density is only 55% that of the bulk. Hence molecules which are deposited on the surface tend to lift the central molecule out of the surface plane, which in turn draws the four corner molecules closer together. Once a sufficiently large number of overlayer molecules has been deposited, vacancies between boundaries between adjacent single crystals must develop. Further deposition results in the filling in of the boundary regions. The extremely close lateral packing of adjacent molecules in a plane results in their mutual vdW core repulsion, thus generating a characteristic tilt of 11° with respect to the substrate plane. This tilt allows for the simultaneous minimization of core repulsion at the molecular edges and molecular attraction between the remaining atoms in the molecule.

As noted in paper I, this preferred alignment between PTCDA and the graphite substrate is a result of the smaller intermolecular compressibility within a layer in contrast to the shear stress between adlayer and substrate. Hence the film is allowed to grow into its preferred, bulk structure without incurring a significant density of defects at the interface. Nevertheless, binding with the substrate is sufficiently strong to ensure that a preferred orientation between the overlayer and substrate lattices is obtained. This process is in contrast to true epitaxy, where the adlayer-substrate shear stress is comparable to the compressibility of the layer itself. In that case, strain between the deposited film and the substrate prohibits crystalline growth beyond one or two monolayers, as has been observed for several cases of molecular crystals tightly bound to the substrate crystal.[5,16]

IV. RHEED OBSERVATION OF THE EVOLUTION OF GROWTH

In past work, RHEED has been used to monitor monolayer growth of such organic crystals as copper phthalocyanine. However, those experiments were performed at anomalously low growth rates of $\sim$0.001 Å/s, and the authors did not report on crystalline growth beyond a monolayer.[16] In contrast, we describe here a series of experiments which provide a direct observation of the *evolution* of PTCDA film nucleation and subsequent growth from monolayer (ML) to multilayer stacks using *in situ* RHEED. In these investigations, RHEED patterns were recorded from a fluorescent screen by a video camera, and saved digitally in a computer for further processing. The energy of the electron beam was 8 keV at a current of $\approx$0.2 mA. The electron beam was directed onto the film surface at an angle of $\sim$2°. After the required film thickness was grown, the shutter to the Knudsen cell was closed to halt further growth, and then the RHEED pattern was obtained by exposing the film to the electron beam. Immediately after recording the RHEED pattern, the beam was directed away from the substrate. We found that leaving the beam on during deposition resulted in the development of broad rings characteristic of amorphous film growth. These features are possibly due to disruption of the grown layer due to charging and/or heating of the relatively insulating films, or even due to damage to the molecules by the high-energy electrons.

A typical series of RHEED patterns obtained during a growth sequence is shown in Fig. 5. At the top left in Fig. 5, we show the RHEED pattern for the bare graphite substrate. From the measured spacing of the streaks and the beam parameters, we calculate a surface unit cell (or surface net) spacing of (2.17$\pm$0.04) Å, which is very close to the predicted (220) reflection of graphite of 2.13 Å. After $\sim$1 Å is indicated on the thickness monitor, the graphite streaks begin to fade, and are completely gone after 1 ML ($\sim$3 Å) of growth. At a film thickness of 10 Å ($\sim$3 ML), the graphite features are replaced by a set of faint doublet streaks as shown in Fig. 5. Most significantly, the appearance of long, continuous streaks is an indication that the first few layers of PTCDA are both crystalline and planar.

As growth proceeds to 20 and 50 Å, the positions of the now intense streaks remain unchanged, although variations in intensity begin to appear at 50 Å along the length of the streaks even though the growth rate has remained at 0.5 Å/s. These RHEED patterns clearly show that the crystalline organic layer retains a high degree of surface planarity and order even though it is not lattice matched to the graphite substrate, which is an indication that quasiepitaxial growth has occurred. As the film thickness is increased to 220 Å, and then finally to

1000 Å, the RHEED pattern periodicity remains unchanged from its value for thinner layers, although the continuous streaks have broken into several segments separated by very faint streak remnants. This streak segmentation is often associated with films that have become uneven on a molecular scale, although their crystalline structure has remained unchanged. An alterative explanation of the discontinuous streaks in the RHEED patterns is that the organic layers are relatively transparent to the high-energy electron beam. Beam penetration to a depth of several layers would therefore result in a three-dimensional diffraction pattern which would be characterized by the discontinuous streaks observed for the thicker layers.

The effect of substrate temperature on film planarity is presented in Fig. 6. This figure compares the RHEED patterns of two 30-Å-thick PTCDA films grown using

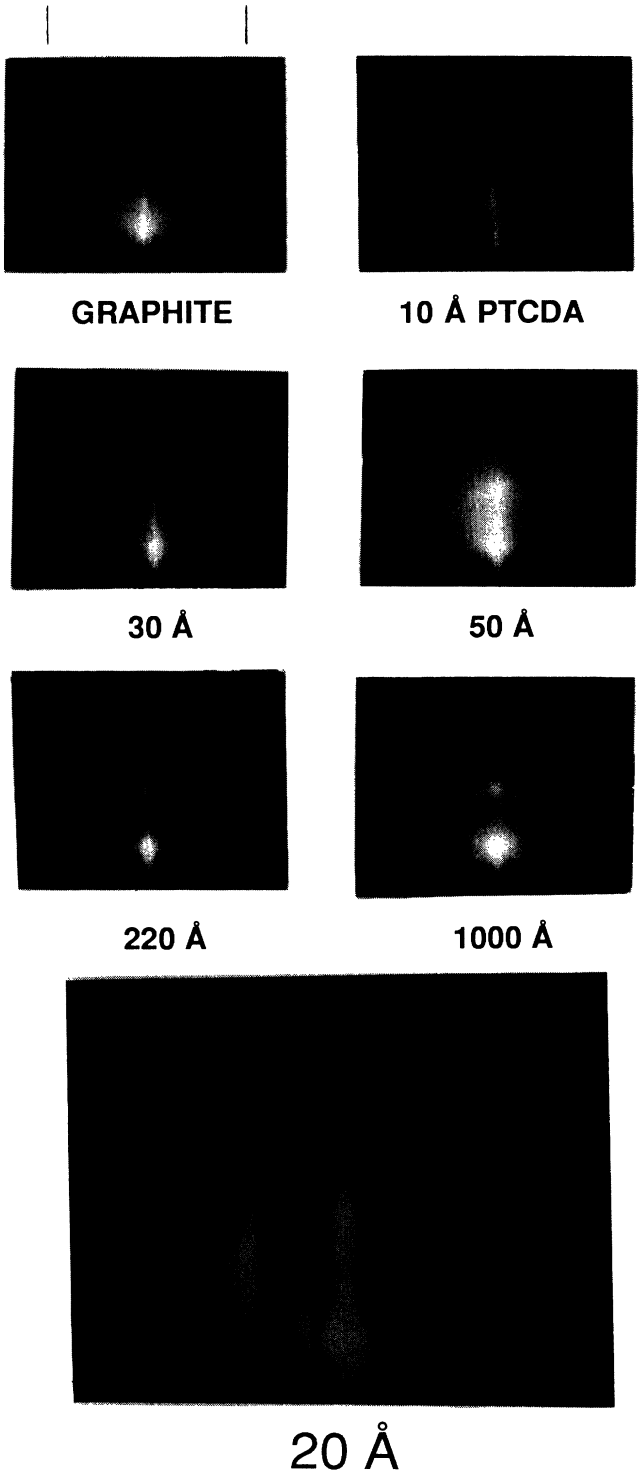

FIG. 5. A series of RHEED patterns obtained for different thicknesses of PTCDA grown on HOPG (whose pattern is shown in the upper left). The 20-Å film RHEED pattern shown at the bottom has been contrast-enhanced to exhibit the detail in the brightest and faintest parts of the pattern.

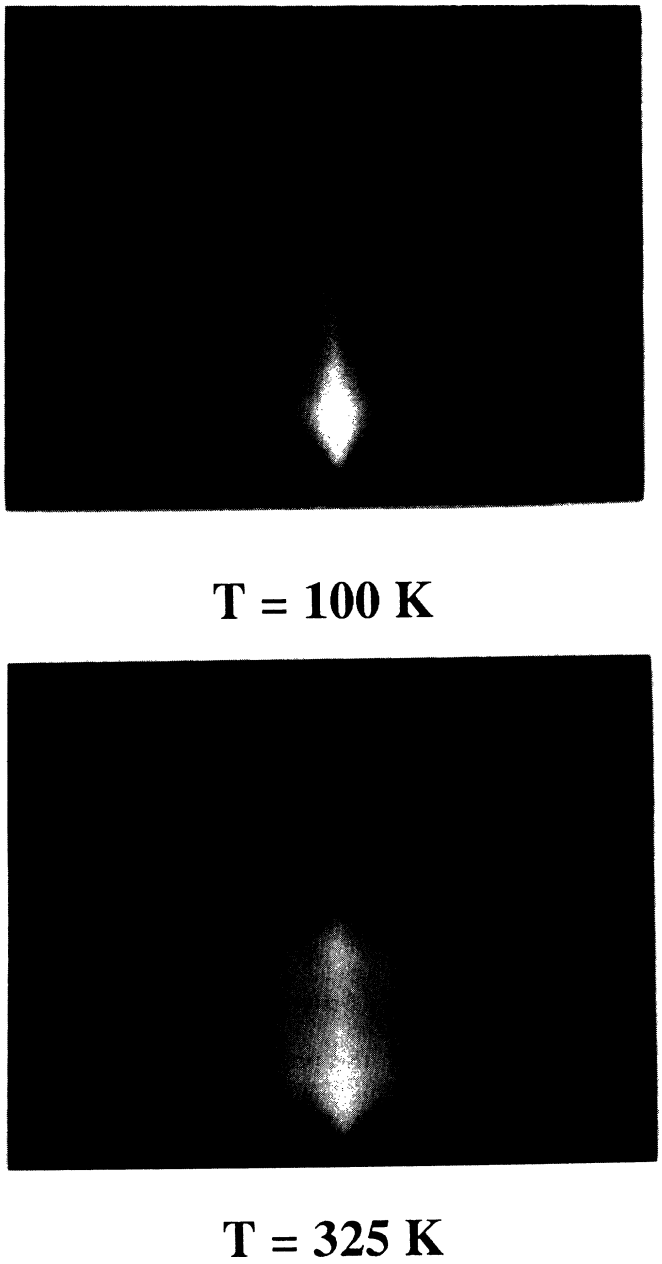

FIG. 6. RHEED patterns obtained for 30-Å-thick PTCDA films grown on a HOPG substrate held at 100 (top) and 325 K (bottom) during growth.

identical conditions, except that the graphite substrate temperature during growth was kept at $T=100$ K in the top image, and at $T=325$ K in the bottom image. Note that the elevated temperature growth results in a somewhat less planar PTCDA surface than for the case of the low-temperature growth. For example, 0.4-μm-thick PTCDA thin films deposited at room temperature at a rate of 3–5 Å/s consist of a mesh of crystalline filaments approximately 0.2 μm long, as indicated in the scanning electron micrograph in Fig. 7(a). These crystalline filaments are oriented randomly on the surface, and hence the resulting film is polycrystalline. On the other hand, for the same films deposited at 90 K [Fig. 7(b)], the surface is smooth, and a uniform crystalline film is achieved. This temperature dependence is a result of thermally induced disorder in high substrate temperature growth, where the vdW bond energy is comparable to the thermal energy of the molecule (see paper I). Low-temperature growth is required to achieve good crystalline order in some films as a result of the relatively weak vdW bond force. Once the entire monolayer is assembled, however, the film structure is stabilized, allowing temperature to be raised without introducing structural disorder or layer decomposition.

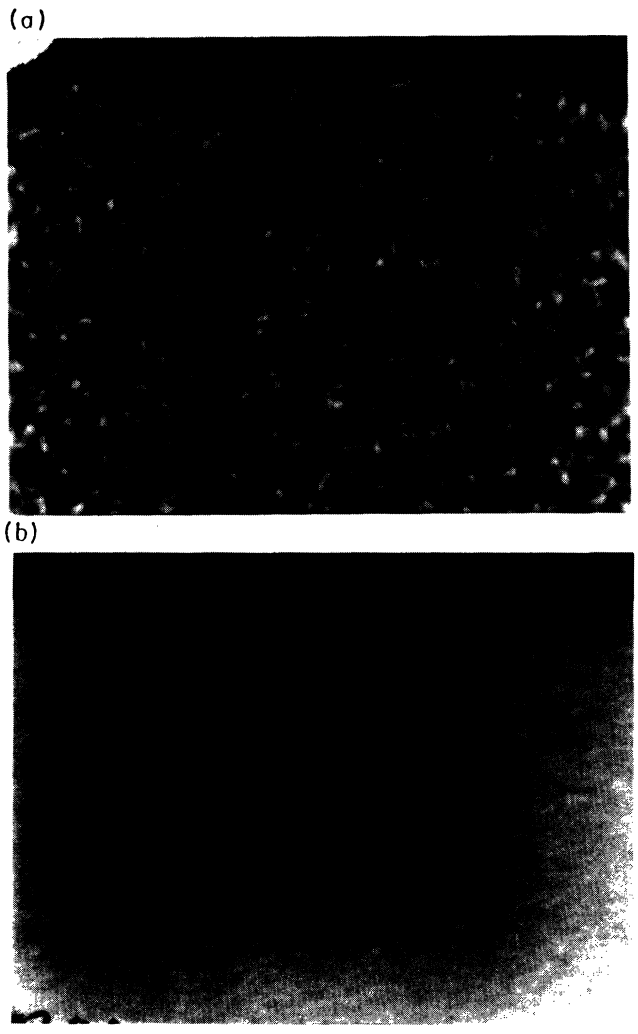

FIG. 7. Scanning electron microscope images of the surface of a PTCDA film grown on glass at a substrate temperature of (a) 293 and (b) 90 K.

Thus far, the discussion has only considered the bright doublet streaks readily apparent in Figs. 5 and 6. However, several less intense reflections are observed from films of thickness ≥ 20 Å. A diagram of all RHEED streaks observed, and their correspondence to a particular crystalline direction, is shown in Fig. 8, where strong reflections are indicated by solid lines and faint reflections by dashed lines. Since the graphite substrate is polycrystalline with a domain size smaller than the area of the electron beam, the reflections of the PTCDA surface unit cell are visible at all substrate orientations.

To identify a particular reflection, we note that the surface unit cell of PTCDA can be approximated as face centered (fc), as inferred from Fig. 3. Here the (01) and (10) reflections, which normally are not allowed for fc cells, are faintly apparent in our RHEED data due to the difference in the molecular form factors of the two, perpendicular-oriented PTCDA molecules in each unit cell. In addition, the strong doublet reflections at (11.2±0.5) and (8.0±0.5) Å correspond to the (02) and (20) reflections from PTCDA since these measurements correspond closely with scanning tunneling microscope measurements made on ML films of PTCDA discussed above. We also observe a streak at (4.0±0.5) Å, corresponding to the (40) reflection, and at (22.4±2) Å, corresponding to the (01) reflection. Two additional streaks are consistent with the (2,2) and (2,4) rods, as shown. A faint, diffuse streak is observed at a spacing of 2.5 Å and is tentatively assigned to the (8,0) rod. The long, continuous streaks observed in the thinnest films in Fig. 5 are indicative of a two-dimensional surface with little or no three-dimensional overgrowth. The appearance of

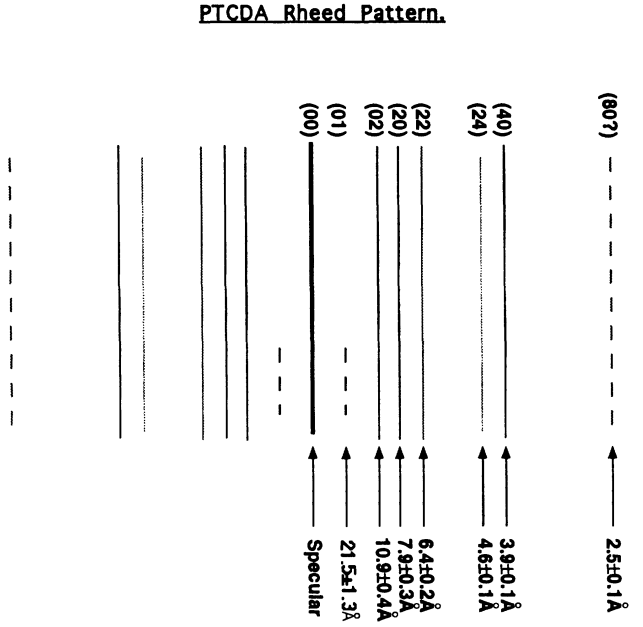

FIG. 8. Schematic representation of a RHEED pattern obtained for PTCDA on HOPG showing the relative spacing of the various diffraction streaks and their crystal structure assignment. Also, the lattice spacing corresponding to each streak is shown.

higher-order diffraction streaks is evidence of the high quality of crystalline growth achievable by quasiepitaxy.

From the above discussion, we conclude that the size of the PTCDA surface unit cell as determined from RHEED is $(21.8\pm0.8)\times(15.8\pm0.6)$ Å^2 (see Table I). This is ~25% larger than the bulk unit-cell dimensions of 17.34×11.96 Å^2. Thus the surface monolayer is reconstructed since it is only bounded by molecules on the bottom plane. We note that this same surface reconstruction has been measured for films up to 1000 Å thick. This strongly suggests that the reconstruction is due to the relatively strong intermolecular forces at the surface of the PTCDA crystal, as opposed to the relatively weak influence of the inorganic substrate.

We extended studies of quasiepitaxial growth of single organic layers[8,17] to examine organic multilayer structures.[18,19] Using RHEED diffraction patterns from a four-layer alternating structure of PTCDA and NTCDA, we find that each layer is crystalline with its own well-defined surface unit cell, regardless of significant lattice mismatch with the underlying layer on which it is deposited. It is clear from Fig. 1 in paper I that it is not possible to achieve lattice matching in the conventional sense due to significant differences in the dimensions and shapes of the two cells.

A typical series of RHEED patterns obtained during the growth of a PTCDA/NTCDA alternating layer structure is shown in Fig. 9. Figure 9(a) shows the pattern resulting from the subsequent deposition of 20 Å (about 3 ML) of NTCDA on 20 Å of PTCDA (cf. Fig. 6) on HOPG, followed by another 20 Å of PTCDA; i.e., a total of 60 Å of organic material. The electron beam was observed to damage the NTCDA layer very rapidly, the streaks fading in only a few seconds. We speculate that this is due to less dense packing and lower molecular weight of the molecules in a crystal of NTCDA (and hence lower vdW bond energy between molecules) than for PTCDA. To ensure a good surface for the growth of the second layer of PTCDA, therefore, the first layer of NTCDA was not exposed to the beam. Streaks corresponding to the (0,2), (2,0), and (4,0) reciprocal-lattice rods for the top PTCDA layer are apparent as in the case for a single-layer PTCDA film, and are measured within experimental error to be at identical spacings to those measured from the first PTCDA layer deposited on HOPG. Clearly, the second layer of PTCDA remains crystalline and two dimensional. Furthermore, the surface unit cell of PTCDA grown on NTCDA is observed to be identical to that of PTCDA grown on HOPG, despite the enormously different lattices of the underlying layers in those two cases. The RHEED pattern from the second layer of PTCDA also indicates that the underlying NTCDA layer is planar, thus resulting in a sharp PTCDA/NTCDA heterointerface.

Figure 9(b) shows the RHEED pattern resulting from the subsequent deposition of a second 20-Å layer of NTCDA; a total of 80 Å of organic film material. It is clearly seen that, as in the case of the other layers, the fourth layer of the organic heterostructure is crystalline, with a radically different RHEED pattern, and hence sur-

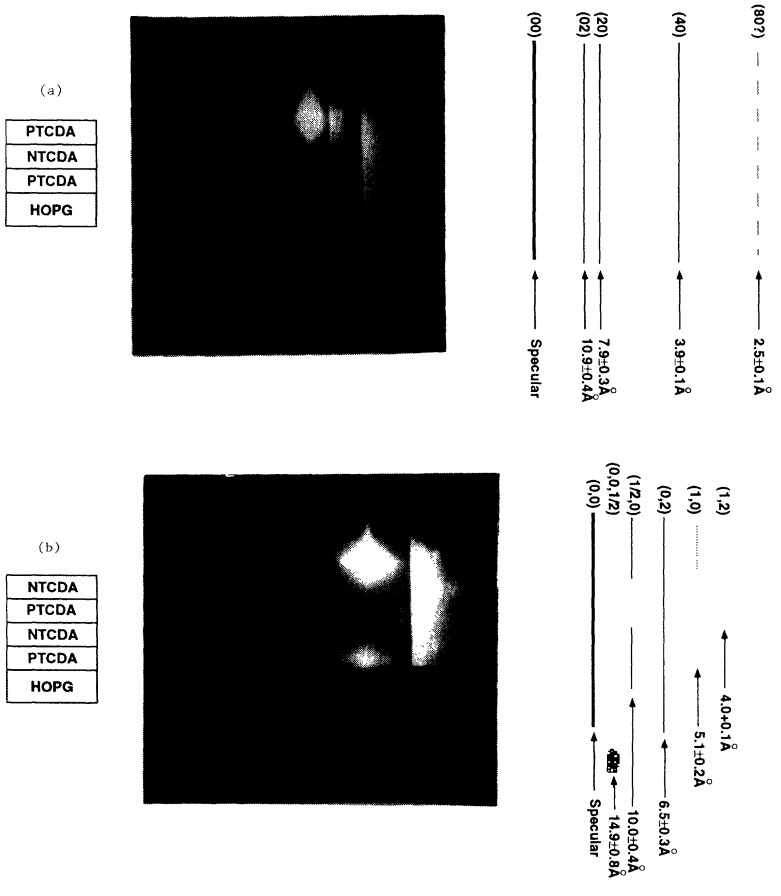

FIG. 9. RHEED pattern of multilayers of PTCDA and NTCDA grown on a HOPG substrate. (a) PTCDA on NTCDA on PTCDA, (b) NTCDA on PTCDA on NTCDA on PTCDA. All layers are 20 Å thick.

face unit cell, to that of PTCDA. Following the example of PTCDA, some surface reconstruction from the bulk lattice spacings is expected. We assign the observed streak at 6.5±0.3 Å to the (0,2) reciprocal-lattice rod of NTCDA. The other streaks are then consistent with the (1,0) rod at 5.1±0.2 Å, and (1,2) at 4.0±0.1 Å, as shown in Fig. 9(b). This, therefore, suggests a reconstructed NTCDA surface unit cell of dimensions 13.0±0.6 ×5.1±0.2 Å^2.

It is also apparent that the herringbone crystal structure of NTCDA will result in some diffraction out of the plane of the substrate even if the layer is completely flat, i.e., the electron beam will provide limited three-dimensional (3D) structural information along the NTCDA *a* axis which will manifest itself as diffuse spots in the diffraction image. This represents a RHEED pattern in which spots from the 3D diffraction and streaks from the 2D diffraction are expected to appear in the same image. Such a phenomenon may explain the diffuse spot at 14.9±0.8 Å below the main diffraction pattern which corresponds to a $(0,0,\frac{1}{2})$ 3D diffraction. The spot cannot be attributed to transmission of the electron beam through clumps of NTCDA on the surface; the planarity of the NTCDA layer is demonstrated by the ability to grow a highly planar layer of PTCDA on its surface.

As an additional example of quasiepitaxial deposition, Fig. 10(a) shows the image from 20 Å of CuPc grown on top of 20 Å of PTCDA on HOPG. The many orders of diffraction visible in the pattern suggest the presence of a crystalline layer of CuPc. A previously published STM image[20] of a monolayer of CuPc on HOPG held at 50 °C suggested a two-dimensional surface unit cell with $b=17.5\pm1$ Å, $c=15.5\pm1$ Å and an angle between the *b* and *c* axes of $\alpha=98\pm1°$. Although the CuPc layer in this report was deposited under different conditions, these parameters may be used as a starting point for interpreting the RHEED streaks. The brightest streaks can be fitted to a surface unit cell with $b=17.5$ Å, $c=13.3$ Å, and $\alpha=98°$. Then the (0,1), (0,2), (1,1), (2,0), and (1,1) rods may be assigned as in Fig. 10(a).

Figure 10(b) shows the RHEED pattern resulting from the deposition of 20 Å of PTCDA on top of the CuPc. The diffuse arcs indicate a layered structure, but no crystalline order within the layers, i.e., no quasiepitaxial deposition is apparent in this third layer. We conclude that the CuPc surface is clearly unsuitable for growth of PTCDA due to three-dimensional growth in the CuPc layer as indicated by the lack of extended streaks in the CuPc RHEED pattern. From these observations, we conclude that although lattice matching is not required, a molecularly flat surface is a necessary condition to achieve quasiepitaxial growth.

V. EFFECTS OF SUBSTRATE TEMPERATURE ON FILM PROPERTIES

In previous x-ray pole figure studies, it was found that single crystalline or twinned films of PTCDA can be

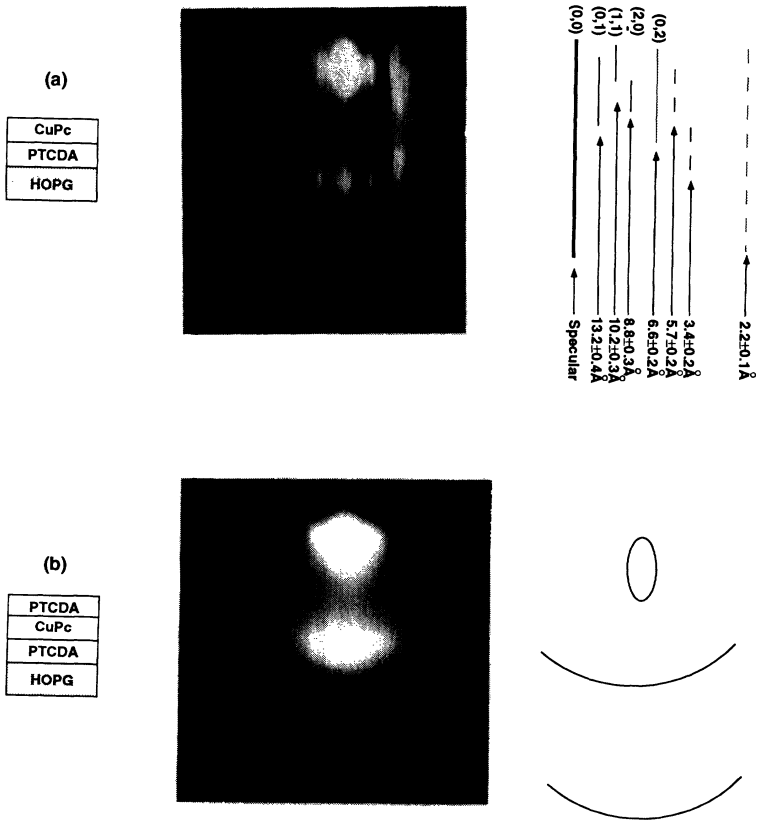

FIG. 10. RHEED pattern of multilayers of PTCDA and CuPc grown on a HOPG substrate. (a) CuPc on PTCDA, (b) PTCDA on CuPc on PTCDA. All layers are 20 Å thick. Note that (b) indicates amorphous growth of the top layer.

achieved on glass substrates under optimized growth conditions.[9] That initial study was, to our knowledge, the first evidence presented for quasiepitaxial growth of large crystallites of a van der Waals-bonded organic molecular thin film on a substrate where no lattice matching can be achieved. That early work was followed by the growth of "approximately" oriented polycrystalline films of PTCDA on amorphous carbon substrates.[21] In the present work, we extend these x-ray investigations to study the substrate temperature dependence of the resulting thin-film microstructure. Figure 11(a) shows the x-ray diffraction patterns (using a Cu $K\alpha$ x-ray source) for 4000-Å-thick PTCDA films deposited on Si wafers at 90 and 293 K, and Fig. 11(b) shows the diffraction patterns for PTCDA films deposited under the same conditions on glass substrates. The diffraction peaks for the samples deposited at 90 K have been shifted along the vertical axis in both figures for clarity. The background intensity observed in Fig. 11(b) is due to x-ray scattering from the glass substrates. For the samples deposited at 293 K, in addition to the prominent (102) diffraction peak, a small (110) peak is also present, indicating the polycrystalline nature of the films. In fact, the (110) peak is observed in all samples deposited at room temperature or above, regardless of the substrate materials used. On the other hand, only one diffraction peak is observed for films deposited on substrates held at 90 K, indicative of the high crystalline order of the PTCDA films. Note that in both samples with Si and glass substrates, the (102) peak intensity of the samples deposited at low temperature is about three times that of the samples deposited at room temperature. The strong diffraction intensity also provides evidence for improved structural ordering in the samples deposited at low temperature.

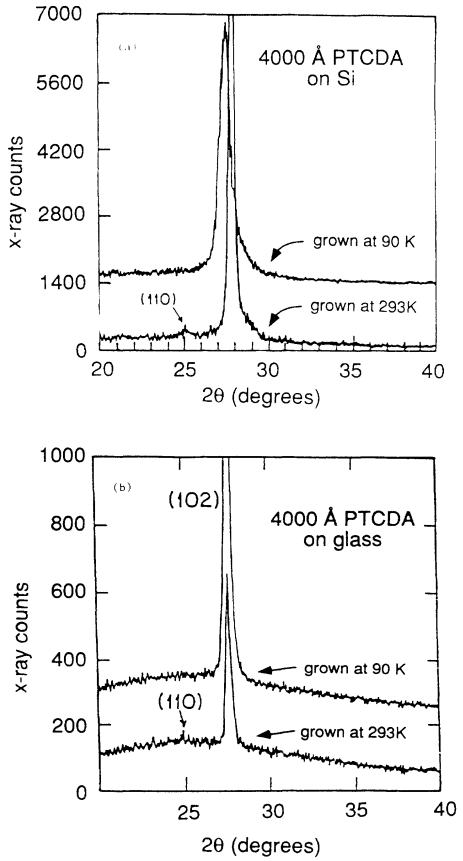

FIG. 11. X-ray diffraction patterns for PTCDA deposited (a) on Si and (b) on glass. The substrate temperature used during growth is indicated in the figure. The strong central peak corresponds to the (102) reflection in PTCDA.

Residual strain is sometimes developed in organic films deposited on Si at low temperatures, as observed by diffraction peak broadening. The full width at half maximum of the (102) diffraction peaks for the Si samples deposited at low temperature is about twice that of the samples deposited at room temperature. Also, there is a slight peak shift in the sample deposited on the Si substrate corresponding to an increase in interplanar spacing of 0.026 Å. Such a shift is not present in the sample deposited on the glass substrate. Both the broadening and shift in the (102) diffraction peak in the low-temperature samples can be explained as follows: Due to the differential thermal expansion in both organic film and substrate, residual stress is developed in the organic films when the sample temperature is brought to room temperature after deposition. Since the thermal expansion coefficient of Si is $2.5\times10^{-6}\,^{\circ}\mathrm{C}^{-1}$, and glass is $5\times10^{-7}\,^{\circ}\mathrm{C}^{-1}$, the residual stress in PTCDA films deposited on Si appears to be larger than that in films deposited on glass. This is also evidenced by cracks which develop in films on Si substrates if the sample temperature is increased back to room temperature too rapidly after growth. On the other hand, cracking is not observed in any samples deposited on glass. As a result of the residual stress in the organic films, inhomogeneous strain causes a slight distortion of the lattice. The fact that the peak shift is not observed in samples deposited on glass substrates also indicates a larger strain in PTCDA films deposited on Si.

When films are deposited at low substrate temperature (<120 K) or high deposition rate (>50 Å/s), it is apparent that molecules stack in a highly ordered fashion. On the other hand, disordered films result when they are deposited at elevated temperatures or low deposition rates. This ordering can also be inferred from the electrical properties of organic/inorganic heterojunctions (OI-HJ). We, therefore, investigated the electrical properties of PTCDA films deposited on Si substrates at various temperatures, and the degree to which their current-voltage (I-V) characteristics are affected by the structural properties of the organic thin films.

In previous work, it has been shown that the I-V characteristics of OI-HJ devices at low current density (J) can be modeled using[9,22]

$$J=J_{s0}[\exp(-qV_d/nkT)-1]\,, \tag{1}$$

which describes thermionic emission current over the barrier at the OI interface. Here V_d is the voltage drop across the heterointerface and is given by $V_d=V_a-V_o$ where V_a is the applied voltage and V_o is the voltage drop across the organic thin film. At low forward bias where J as described in Eq. (1) is small, then $V_d\approx V_a$.

Also, q is the electronic charge, $n \approx 2$ is the ideality factor, and kT is the thermal energy at temperature T. As has been shown previously, J_{s0} is the saturation current which is a function of the OI-HJ energy barrier height.[22]

At high forward current density, carrier transport is dominated by space-charge effects in the organic film, in which case $V_o = V_a - V_d$, and

$$J = [\tfrac{9}{8}]\varepsilon\mu V_o^2/d^3 , \quad (2)$$

where μ is the majority carrier mobility in the organic thin film, ε is the permittivity, and d is the film thickness. Hence, by measuring $J(V)$ at high current densities where $J(V) \sim V^2$, we can determine the carrier mobility. Then, by correlating mobility with film growth conditions we can qualitatively infer the degree of stacking order on these growth parameters since μ is ultimately determined by the π-bond overlap between molecules in the stack.

To fabricate OI diodes, indium was first deposited onto the back side of p-Si substrates (with substrate resistivity of 5 Ω cm), then the wafers were degreased by standard organic solvents. The surface oxide was removed immediately prior to film growth by immersion of the wafer in a dilute HF solution. Next, PTCDA films with thicknesses ranging from 500 to 4000 Å were deposited at a rate of 5–10 Å/s onto the top wafer surface followed by indium contact deposition through a shadow mask onto the organic films. The metal contact area was 5.5×10^{-4} cm^2. Electrical measurements of the OI-HJ diodes were made using fine gold wire probes to avoid damage to the thin films.

Figure 12 shows the forward current-voltage (I-V) characteristics for OI-HJ devices with 2000-Å-thick PTCDA films deposited at different substrate temperatures. For the sample with the organic film deposited at 90 K, the forward current has an exponential dependence on voltage due to diffusion current across the OI heterointerface in the low bias voltage regime [Eq. (1)], and then exhibits a roll off in current due to space-charge-limited current at large bias voltages [Eq. (2)]. For the sample with PTCDA deposited at 443 K, the forward current has no exponential dependence for the entire voltage range studied. This indicates low carrier mobility in the organic film. Fits to the experimental I-V data using analyses of the dark current discussed above are also shown by the solid lines in Fig. 12. From these fits, we find that the carrier mobility in the organic films decreases from 0.16 cm^2/V s for the sample deposited at 90 K to 2×10^{-4} cm^2/V s for the sample deposited at 443 K.

Figure 13 shows the carrier mobility for PTCDA films of different thicknesses deposited at various temperatures. Note that the carrier mobility is highest for films deposited at 90 K, and decreases as the deposition temperature increases, except for the 500-Å sample. As shown in Fig. 13, there is no difference in carrier mobility between the 500-Å-thick samples deposited at 90 and 293 K. For the 500-Å sample deposited at 443 K, however, the carrier mobility decreases by about two orders of magnitude compared to the samples deposited at lower temperatures. A similar trend is also observed in the 1000-Å sample, where there is only a small difference in mobility between the samples deposited at 90 and 293 K. In contrast, the carrier mobilities of the thicker samples (2000 and 4000 Å) deposited at 90 and 293 K differ by about two orders of magnitude.

The results of the mobility measurements of organic films can be explained in terms of their structural properties. For PTCDA films deposited at low temperatures or high deposition rates, molecules form stacks tilted at an angle of 11° from the substrate normal, resulting in large π-orbital overlap along the c axis in the unit cell (see Fig. 1 of paper I). Charge carriers in the organic films can therefore move along the stacking direction, giving rise to high carrier mobility in the films. On the other hand, films deposited at elevated temperatures are polycrystalline with randomly oriented molecular stacks. This disorder results in a reduction in orbital overlap between molecules normal to the substrate, thereby reducing the carrier mobility in this direction by almost four orders of magnitude in some cases. Disorder in the stacks leads to a reduction of the π-orbital overlap between molecules, thereby decreasing the mobility of charge along the stacking direction. Note that while we can infer informa-

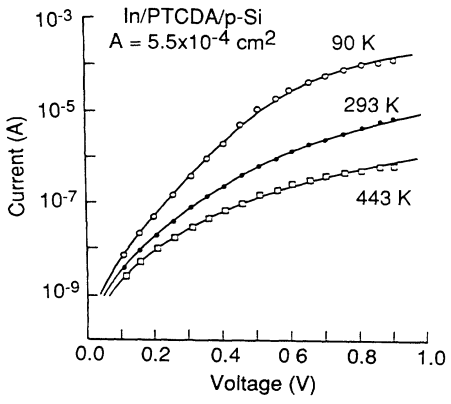

FIG. 12. Forward-biased current-voltage characteristics for In/2000-Å PTCDA/p-Si devices where the organic layer was deposited at different temperatures indicated. Solid lines are fits to the data using theory described in text.

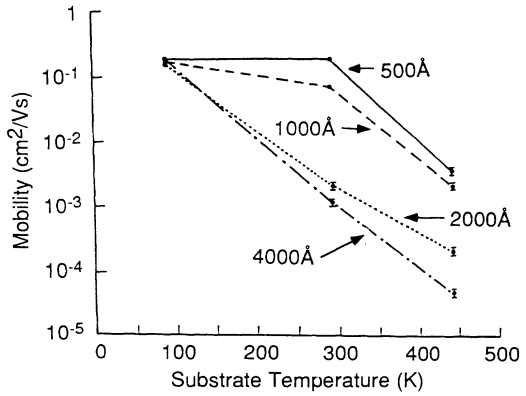

FIG. 13. Hole mobility in the PTCDA layer as a function of PTCDA film deposition temperature. The mobilities are obtained from fits to current-voltage data for films of different thicknesses.

tion about the stacking order from these mobility measurements, they provide no information about the order within the plane of the film (and hence the molecular plane). This results since mobility in the plane is extremely small[9] as a result of negligible in-plane π-system overlap between molecules.

In addition to the substrate temperature dependence on the carrier mobility in organic films, the mobility also has a thickness dependence for films deposited at elevated temperatures (293 and 443 K). Except for the films deposited at 90 K, as the thickness of the film increases, the mobility decreases. Such a thickness dependence is also apparent in the surface morphologies of PTCDA films deposited at room temperature. For example, for a 500-Å sample deposited at room temperature, no surface texture is observed, indicating a strong structural ordering which accounts for the high carrier mobility. On the other hand, for a 2000-Å-thick film deposited at room temperature, considerable surface texture is observed indicating the polycrystalline nature of the films which give rise to a reduction in carrier mobility.

VI. EFFECTS OF ORDER ON FILM DIELECTRIC PROPERTIES

One consequence of anisotropic crystal structure in a thin film is that the films exhibit enormous anisotropies in both their conductive and dielectric properties. For example, the in-plane conductivity of PTCDA films is found to be at least six orders of magnitude lower than the conductivity perpendicular to the film plane.[9] It is also expected that the dielectric properties of highly ordered films would have a considerable degree of anisotropy along different crystalline directions. The off-resonance dielectric constant of a material at frequency, ω, is given by

$$\varepsilon - 1 = \frac{4\pi N q^2 f_j}{m^*(\omega_j^2 - \omega^2)} , \tag{3}$$

where N is the molecular number density, ω_j is the dipole transition frequency, q is the electronic charge, and m^* is the electron effective mass. The oscillator strength of the dipole transition from level o to j is given by $f_j = 2m^* h\omega |x_{oj}|^2/\hbar^2$, where x_{oj} is the electron position expectation value, and $\hbar$ is Planck's constant divided by 2π. Assuming that the largest contribution to the dipole moment of the molecule is due to the π orbitals, and that the electron within a given orbital is completely delocalized, then we can make the approximation that $f_{j\perp}/f_{j\parallel} \sim |x_{oj\perp}|^2/|x_{oj\parallel}|^2 \sim d^2/L^2$. For the case of PTCDA, $d \simeq 3.2$ Å is the extent of the π-orbital system perpendicular to the molecular plane, and L is its extent in the plane, which is approximately equal to the length of the perylene molecular core of PTCDA (i.e., $L \simeq 6.9$ Å). Hence, provided that there is perfect crystalline alignment throughout the QE film, we can expect an anisotropy in ε between directions perpendicular and parallel to the thin-film plane (and hence approximately perpendicular and parallel to the molecular stacking axis) of $(\epsilon_\perp - 1)/(\varepsilon_\parallel - 1) \sim d^2/L^2 \sim 0.22$. This value is only an approximation, since we are assuming that m^* is isotropic, and that the dipole moment is due to a completely delocalized electron in the extended π system. Nevertheless, it has been found[23] that the measured value of $(\varepsilon_\perp - 1)/(\varepsilon_\parallel - 1) = 0.26$ for PTCDA, which is close to the value predicted by the above model. Furthermore, the index of refraction measured at a wavelength of $\lambda = 1.064$ μm in the direction perpendicular to the substrate plane is $n_\perp = 1.36 \pm 0.01$, whereas parallel to the plane, $n_\parallel = 2.017 \pm 0.005$, resulting in an index difference (or birefringence) of $\Delta n = 0.66$. To our knowledge, these are the largest index anisotropies ever measured for thin films, giving further evidence for the nearly perfect crystalline order achieved in QE growth.

Finally, further evidence for the high crystalline order of OMBD-grown PTCDA films has been obtained by measuring optical propagation loss in PTCDA waveguides. In recent experiments, we have found that such waveguides deposited on polyimide buffer layers[24] (with $n_{\text{buffer}} = 1.6$) have losses less than 1 dB/cm for TE-polarized light, although extremely high losses were measured for TM propagation. The low loss for TE waves indicates that there is a low density of grain boundaries which would result in scattering losses. Scattering from grain boundaries, which is commonly observed in polycrystalline waveguides has two effects which lead to severe propagation loss: (i) outcoupling from waveguide surfaces; and (ii) scattering of TE into TM modes, which are extremely lossy in waveguides where $n_{\text{TM}} \simeq n_\perp < n_{\text{buffer}}$, as is the case of the waveguides studied in Ref. 24. While this result provides only inferential evidence for the high degree of crystalline order of the films, it nevertheless suggests that the number of grain boundaries in waveguides whose length exceeds 7 mm is very small, and that the optic axis is oriented such that its projection is along the waveguiding direction (since other orientations would lead to rotation of the TE-mode propagation, and hence large optical loss). Since the optic axis has a fixed orientation with respect to the unit cell, we therefore conclude that the molecules with the thin-film waveguide must all be approximately oriented in the same direction relative to each other and the buffer layer. This approximate orientation therefore strongly suggests uniform, quasiepitaxial growth of the organic thin film.

VII. DISCUSSION AND CONCLUSIONS

We have discussed several aspects of film growth, from the monolayer to the bulk thin-film stage indicating that archetype planar molecules such as PTCDA and NTCDA can indeed be grown in crystalline form on a variety of substrates. Structural data obtained from monolayer and multilayer thin-film stacks indicate ordering into structures which are consistent with predictions made using the simple model describing quasiepitaxial growth presented in paper I. For example, both the expanded surface unit cell and orientation with respect to the graphite substrate predicted in the molecular theory in paper I have been observed using a combination of RHEED and STM measurements. The structural ordering is maintained well beyond the monolayer stage, to

films exceeding 2000 Å in thickness. The cell dimensions and angles measured using the several techniques discussed in this paper for monolayer and bulk forms of OMBD-grown PTCDA are summarized in Table I. We also provide the theoretically predicted values[1] for these dimensions in the table. The good agreement between theory and measurement indicates that the fundamental assumptions regarding quasiepitaxial growth (i.e., that the interlayer compressibility be much larger than the compressibility within a layer) are supported by observation for large, planar, van der Waals-bonded molecular solids such as PTCDA and NTCDA. These theoretical predictions have also been extended to the growth of two dissimilar organic molecules. The experiments presented here on multilayer stacks of PTCDA on NTCDA also provide evidence to support our theoretical results.

We also provide evidence that the high degree of ordering strongly influences such macroscopic film properties as optical birefringence, the pronounced anisotropy in the dielectric and conductive properties of the films, film morphology, and carrier mobility.

Taken in the context of a growing body of evidence for QE growth of a large number of molecular species on a wide variety of substrates presented here and by others, it is apparent that QE growth of van der Waals-bonded planar organic molecules is a general property of these materials systems. Since this property has been shown to strongly influence the macroscopic optoelectronic film properties, quasiepitaxially grown organic thin films may open the way to an unprecedented range of applications in photonics and electronics.

ACKNOWLEDGMENTS

The authors thank Dr. D. Y. Zang for measurements on the dielectric properties of the thin films. Also, we thank the Air Force Office of Scientific Research (G. Pomrenke and C. Lee), Rome Air Development Center (J. Lorenzo), and ARPA (A. Yang) for their support of this research. In addition, E.I.H. thanks Rockwell International Corp. for support through the University of Southern California.

---

*Currently on leave from the University of Southern California, Los Angeles, CA 90089.

†Currently with Motorola, Inc., Tempe, AZ.

[1]S. R. Forrest and Y.-Z. Zhang, preceding paper, Phys. Rev. B **49**, 11 297 (1994).

[2]Aldrich Chemical Company, Milwaukee, WI.

[3]F. Gutmann and L. E. Lyons, *Organic Semiconductors* (Wiley, New York, 1967).

[4]K. Tanigaki, S. Kuroshima, T. W. Ebbesen, and T. Ichihashi, Mol. Cryst. Liq. Cryst. Sci. Technol. B: Nonlinear Opt. **2**, 179 (1992).

[5]M. Hara, I. Iwakabe, H. Sasabe, A. Yamada, and A. F. Garito, Nature **344**, 228 (1990).

[6]P. H. Lippel, R. J. Wilson, M. D. Miller, Ch. Woll, and S. Chiang, Phys. Rev. Lett. **62**, 171 (1989).

[7]C. Ludwig, B. Gompf, W. Glatz, J. Petersen, W. Eisenmenger, M. Mobus, U. Zimmermann, and N. Karl, Z. Phys. B **86**, 397 (1992).

[8]P. E. Burrows, Y. Zhang, E. I. Haskal, and S. R. Forrest, Appl. Phys. Lett. **61**, 2417 (1992).

[9]S. R. Forrest, M. L. Kaplan, and P. H. Schmidt, J. Appl. Phys. **55**, 1492 (1984).

[10]T. Minakata, H. Imai, M. Ozaki, and K. Saco, J. Appl. Phys. **72**, 5220 (1992).

[11]S. Cincotti and J. B. Rabe, Appl. Phys. Lett. **62**, 3531 (1993).

[12]M. K. Debe and D. R. Field, J. Vac. Sci. Technol. A **9**, 1265 (1991).

[13]F. F. So, L. Y. Leu, and S. R. Forrest, in *Growth of Semiconductor Structures and High-T_c Thin Films on Semiconductors,* edited by A. Madhuka, Proc. SPIE No. 1285 (SPIE, Bellingham, 1990), p. 95.

[14]Nanoscope II, Digital Instruments, Inc., Santa Barbara, CA 93110.

[15]Materials Analytical Services, Raleigh, NC 27607.

[16]M. Hara, H. Sasabe, A. Yamada, and A. F. Garito, Jpn. J. Appl. Phys. **28**, L306 (1989).

[17]E. I. Haskal, F. F. So, P. E. Burrows, and S. R. Forrest, Appl. Phys. Lett. **60**, 3223 (1992).

[18]P. E. Burrows and S. R. Forrest, Appl. Phys. Lett. **62**, 3102 (1993).

[19]F. F. So, S. R. Forrest, Y. Q. Shi, and W. H. Steier, Appl. Phys. Lett. **56**, 674 (1990).

[20]P. E. Borrows, M. Hara, and H. Sasabe, Mol. Cryst. Liq. Cryst. Sci. Technol. B: Nonlinear Opt. **2**, 193 (1992).

[21]A. J. Lovinger, S. R. Forrest, M. L. Kaplan, P. H. Schmidt, and T. Venkatesan, J. Appl. Phys. **55**, 476 (1984).

[22]S. R. Forrest and F. F. So, J. Appl. Phys. **64**, 399 (1988).

[23]D. Y. Zang, F. F. So, and S. R. Forrest, Appl. Phys. Lett. **59**, 823 (1991).

[24]D. Y. Zang, Y. Q. Shi, F. F. So, S. R. Forrest, and W. H. Steier, Appl. Phys. Lett. **58**, 562 (1991).

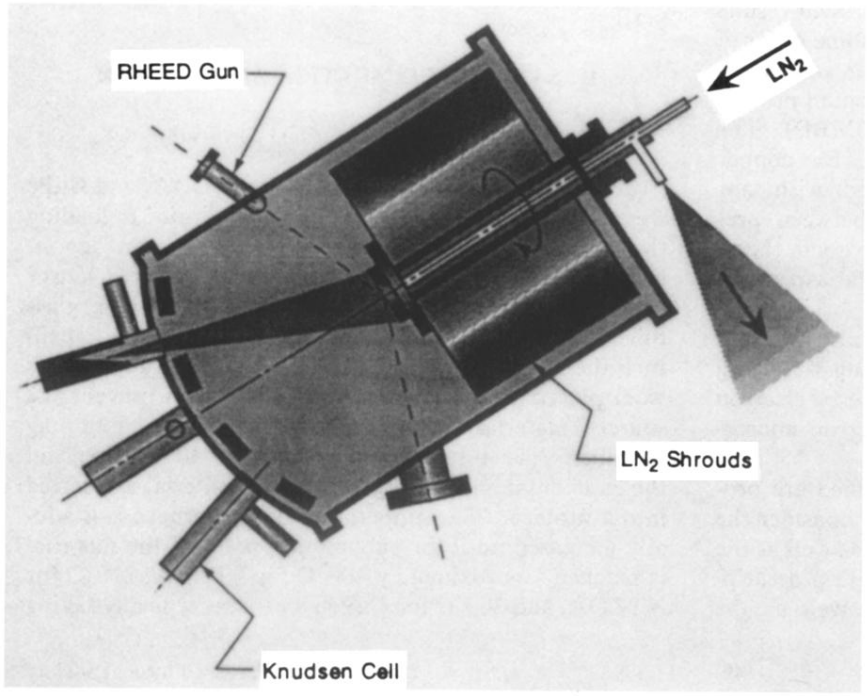

FIG. 1. Cross-sectional view of the organic molecular-beam deposition chamber. The rotating substrate holder can be temperature controlled between 80 and 900 K using a combination of liquid-nitrogen-cooling and boron-nitride-heating elements.

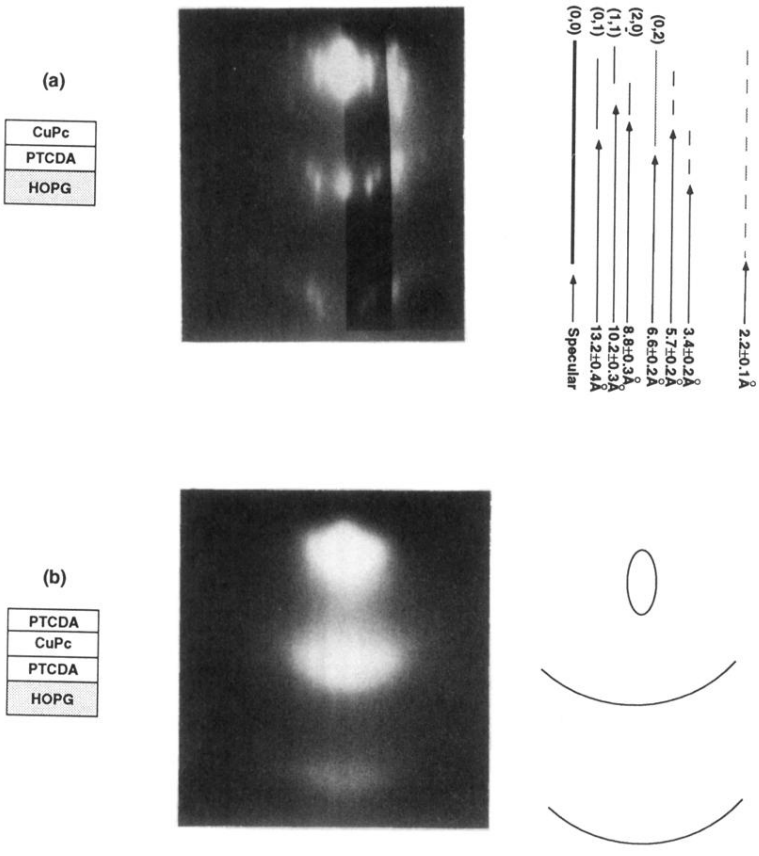

FIG. 10. RHEED pattern of multilayers of PTCDA and CuPc grown on a HOPG substrate. (a) CuPc on PTCDA, (b) PTCDA on CuPc on PTCDA. All layers are 20 Å thick. Note that (b) indicates amorphous growth of the top layer.

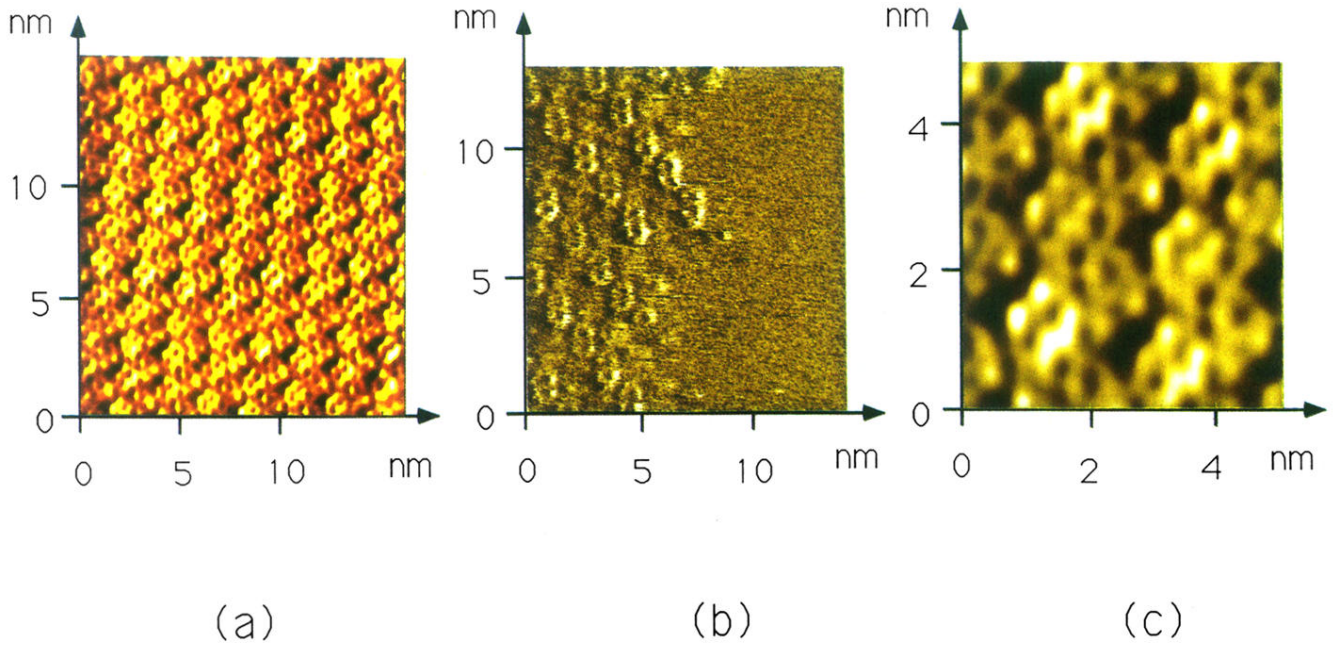

FIG. 2. (a) False color filtered STM image of crystalline PTCDA on HOPG. Tip operating parameters: 402.1-mV, 0.10-nA tip positive. (b) Unfiltered STM image of the edge of an island of PTCDA on HOPG. Tip operating parameters: 403.7-mV, 0.10-nA tip positive. (c) Detail of (a), showing the unit cell of PTCDA on HOPG.

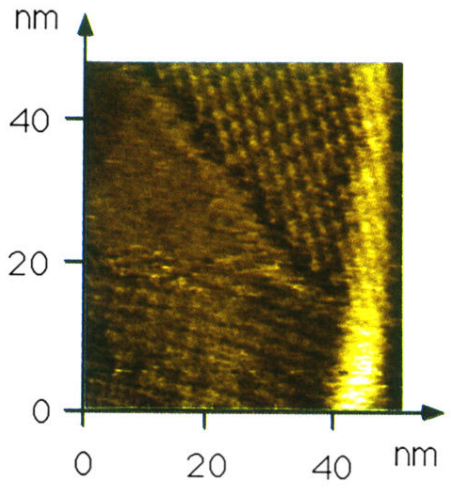

FIG. 4. STM image of two crystalline grains of PTCDA on a HOPG substrate. The space in the center of the "*V*" between the grains is a region where no PTCDA growth has occurred.

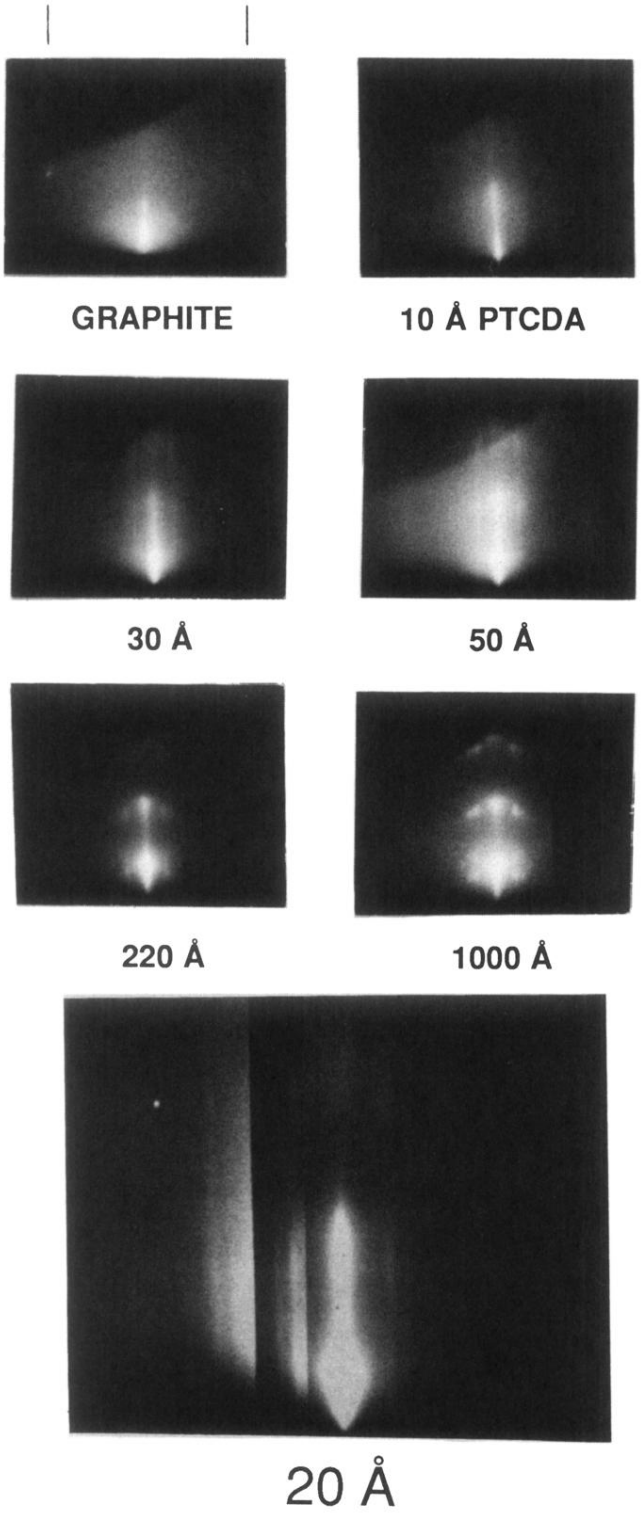

FIG. 5. A series of RHEED patterns obtained for different thicknesses of PTCDA grown on HOPG (whose pattern is shown in the upper left). The 20-Å film RHEED pattern shown at the bottom has been contrast-enhanced to exhibit the detail in the brightest and faintest parts of the pattern.

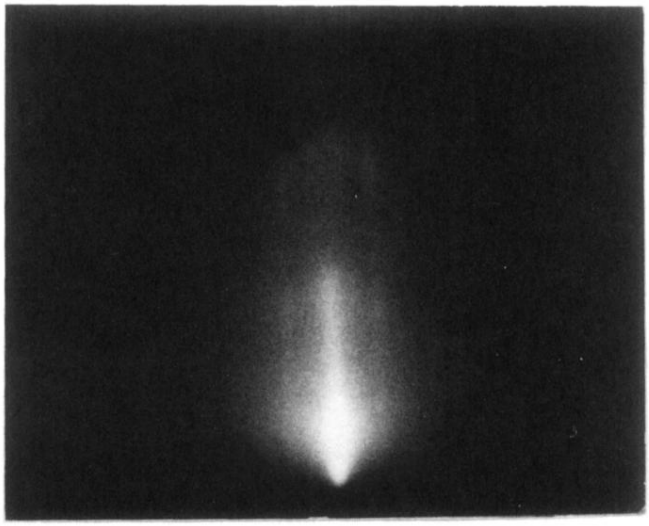

T = 100 K

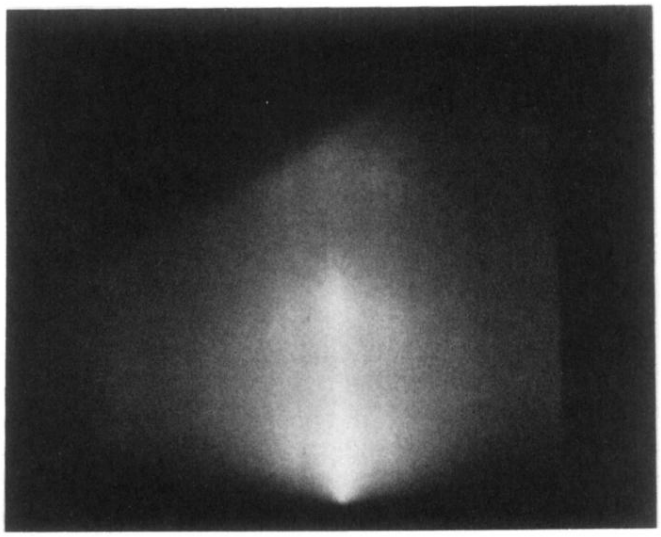

T = 325 K

FIG. 6. RHEED patterns obtained for 30-Å-thick PTCDA films grown on a HOPG substrate held at 100 (top) and 325 K (bottom) during growth.

(a)

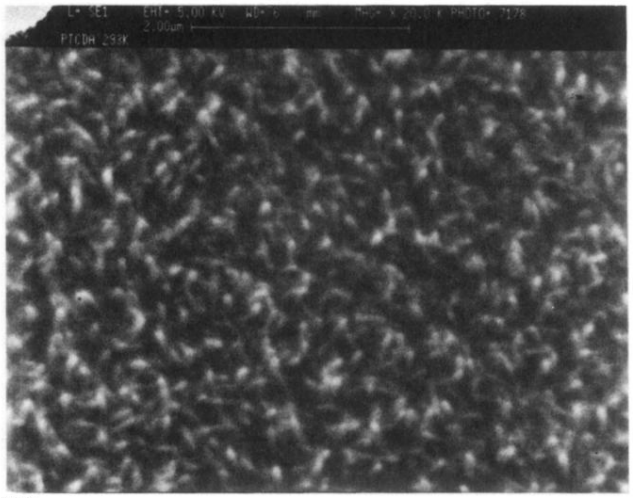

(b)

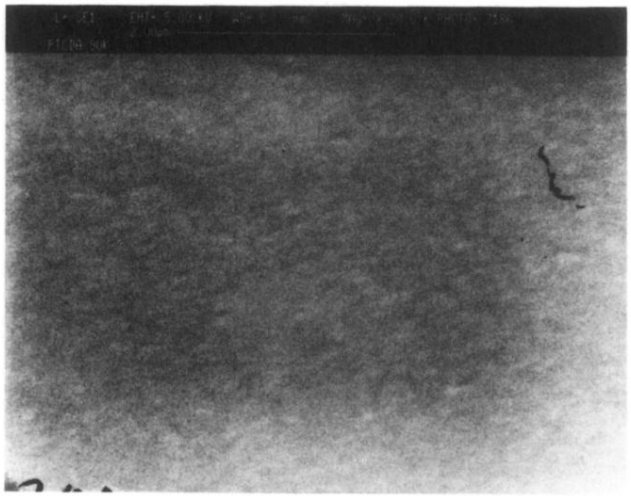

FIG. 7. Scanning electron microscope images of the surface of a PTCDA film grown on glass at a substrate temperature of (a) 293 and (b) 90 K.

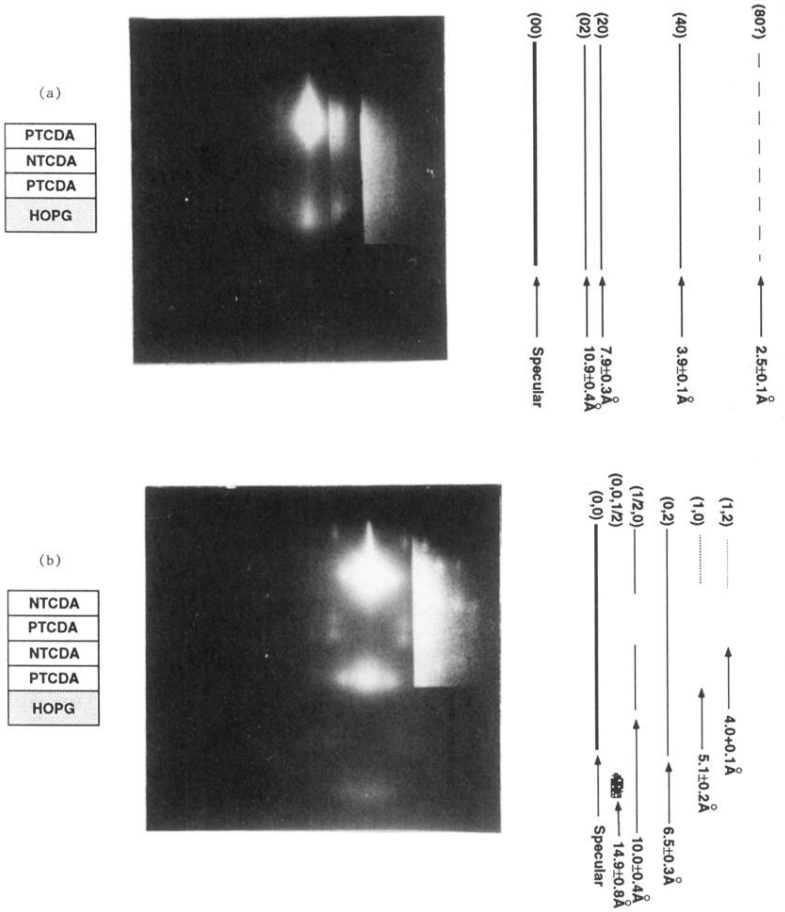

FIG. 9. RHEED pattern of multilayers of PTCDA and NTCDA grown on a HOPG substrate. (a) PTCDA on NTCDA on PTCDA, (b) NTCDA on PTCDA on NTCDA on PTCDA. All layers are 20 Å thick.